

Preparation, Characterization, Molecular and Electronic Structures, TDDFT, and TDDFT/PCM Study of the Solvatochromism in Cyanovinylferrocenes

Victor N. Nemykin,^{*†} Elena A. Makarova,^{†‡} Jeffrey O. Grosland,[†] Ryan G. Hadt,[†] and Alexey Y. Kopusov[†]

Department of Chemistry and Biochemistry, 1039 University Drive, University of Minnesota, Duluth, Minnesota 55812, and Organic Intermediates and Dyes Institute, 1/4 B. Sadovaya Street, Moscow, 103787, Russia.

Received March 23, 2007

Cis and trans isomers of ferrocene-based donor–acceptor assemblies, Fc–C(l)=CH(l), Fc–C(l)=CH(CN), and Fc–C(CN)=CH(CN) (Fc is ferrocene), along with the Fc–C(CN)=C(CN)₂ complex have been prepared and characterized by ¹H, ¹³C, gHMQC, and gHMBC NMR spectra, IR, UV–vis, and MCD spectroscopy methods, as well as elemental analyses. The oxidation potentials, investigated by cyclic voltammetry, of all donor–acceptor assemblies are in agreement with the electron-acceptor strength of the substituents attached to the ferrocene core. X-ray crystallography studies of cis and trans isomers of Fc–C(l)=CH(CN) and Fc–C(CN)=CH(CN) reveal a significant rotational flexibility of the cyanovinyl group, which was explained on the basis of semiempirical PM3 calculations. Electronic structures and solvatochromic properties of all complexes were investigated by UV–vis spectroscopy, density functional theory (DFT), time-dependent DFT (TDDFT), and polarized continuum model (PCM) TDDFT approaches. The calculated vertical excitation energies and magnitudes of solvatochromic effect are consistent with the experimental data and clearly suggest the dominance of metal-to-ligand charge-transfer bands in the visible region of the UV–vis spectra for all complexes.

Introduction

Metalloocene-, and in particular, ferrocene-based donor–acceptor chromophoric assemblies are widely investigated because of their potential application in nonlinear optics.¹ In addition, ferrocene-based chromophores possess very interesting solvatochromic properties, and the influence of the electronic structure of the donor and acceptor parts of the donor–acceptor assemblies on the optical properties of

these conjugated metallocenes was widely discussed in the literature.^{2–4} Very recently, it was shown that the conjugated ferrocenylspiropyranes can act as controllable molecular photomemory elements.⁵ Cyanovinyl substituents were proven to be among the best acceptor groups controlling solvatochromic properties of different ferrocene-based donor–acceptor chromophores.^{3,6} We have recently shown that the coupling of parent ferrocene with a tricyanovinyl group results in the very strong solvatochromic properties of tricyanovinylferrocene.⁶ In this paper, we would like to systematically investigate the influence of the number of cyano groups and their positions (i.e., cis vs trans) on redox and solvatochromic properties of mono- (*cis-3* and *trans-3*) di- (*cis-4* and *trans-4*) and tri- (*5*) cyanovinylferrocenes

* To whom correspondence should be addressed. E-mail: vnemykin@umn.edu.

[†] University of Minnesota.

[‡] Organic Intermediates and Dyes Institute.

- (1) (a) Long, N. *J. Angew. Chem., Int. Ed. Engl.* **1995**, *34*, 21. (b) Stankovic, E.; Toma, S.; Van Boxel, R.; Asselberghs, I.; Persoons, A. *J. Organomet. Chem.* **2001**, *426*, 637.
- (2) (a) Barlow, S.; Marder, S. *Chem. Commun.* **2000**, 1555. (b) Laus, G.; Strasser, C. E.; Holzer, M.; Wurst, K.; Pürstinger, G.; Ongania, K.-H.; Rauch, M.; Bonn, G.; Schottenberger, H. *Organometallics* **2005**, *24*, 6085. (c) Pizzoti, M.; Ugo, R.; Dragonetti, C.; Annoni, E. *Organometallics* **2003**, *22*, 4001. (d) Flood, A. H.; McAdam, C. J.; Gordon, K. C.; Kjaergaard, H. G.; Manning, A. M.; Robinson, B. H.; Simpson, J. *Polyhedron* **2007**, *26*, 448. (e) Kunkely, H.; Vogler, A. *J. Organomet. Chem.* **2001**, *637*, 777.

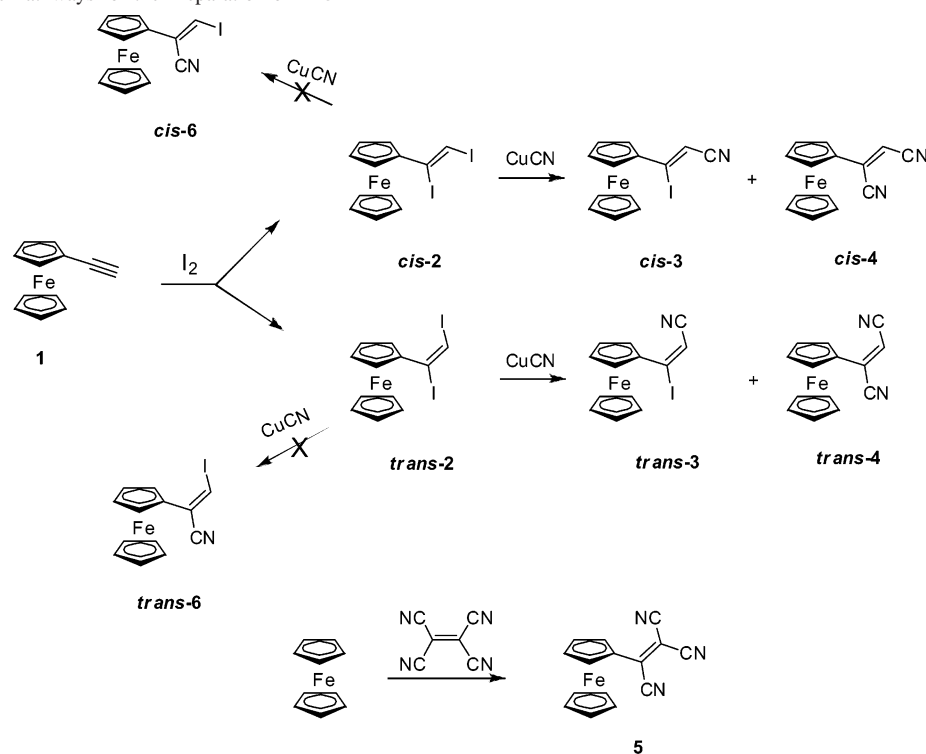
(3) Laus, G.; Schottenberger, H.; Schuler, N.; Wurst, K.; Herber, R. H. *J. Chem. Soc., Perkin Trans.* **2002**, *2*, 1445.

(4) Laus, G.; Schottenberger, H.; Wurst, K.; Herber, R. H.; Griesser, U. *J. Phys. Chem. B* **2004**, *108*, 5082.

(5) Nagashima, S.; Murata, M.; Nishihara, H. *Angew. Chem., Int. Ed.* **2006**, *45*, 4298.

(6) Nemykin, V. N.; Maximov, A. Y.; Kopusov, A. Y. *Organometallics* **2007**, *26*, 3138.

Scheme 1. Synthetic Pathways for the Preparation of 2–5



presented in Scheme 1 along with diiodovinylferrocenes (*cis*-2 and *trans*-2).

Experimental Section

Materials and Physical Measurements. All reactions were performed under a dry nitrogen or argon atmosphere with flame-dried glassware. Ethynylferrocene, iodine, copper(I) cyanide, potassium iodide, sodium thiosulfate, sodium sulfate, magnesium, ferrocene, and tetracyanoethylene were purchased from commercial sources and used without further purification. Diethyl ether and dimethylformamide (DMF) were dried over molecular sieves (4 Å), while dry acetonitrile was obtained by distillation over calcium hydride. All solvents used in column chromatography, UV–vis spectroscopy, and reaction workups were purchased from commercially available sources and used without further purification. Silica gel (60 Å, 32–63 mesh) was purchased from Sorbent Technologies. Tetrabutylammonium perchlorate (TBAP) was recrystallized twice from ethyl acetate prior to use in electrochemical experiments. NMR spectra were recorded on a Varian Unity INOVA instrument with a 500 MHz frequency for protons and 125 MHz for carbon. Chemical shifts are reported in ppm and referenced to TMS as an internal standard. UV–vis data were obtained on HP 8453 or Cary 17 spectrophotometers. MCD data were recorded using an OLIS DSM 17 CD spectropolarimeter using a constant field (1.4 T) DeSa magnet. IR spectra were recorded using a Perkin-Elmer FT-IR 1760X spectrometer in KBr pellets. Elemental analysis was done at Atlantic Microlab Inc. (Atlanta). Electrochemical measurements were conducted using a CH electrochemical analyzer utilizing a three-electrode scheme with platinum working and auxiliary electrodes and a Ag/AgCl reference pseudo-electrode in a 0.1 M solution of TBAP in acetonitrile with redox potentials corrected using an internal standard (ferrocene) in all cases.

Synthesis. (*Z*)- and (*E*)-1,2-Diiodo-1-ferrocenylethylenes (*cis*-2 and *trans*-2). A mixture of 1.0 g (4.76 mmol) of ethynylferrocene, 3.02 g (11.9 mmol) of iodine, and 1.98 g (11.9 mmol) of potassium

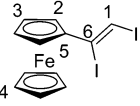
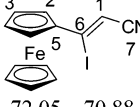
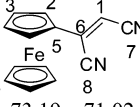
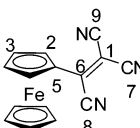
Table 1. ¹H NMR Peak Assignments in 2–5

complex	α-Cp H2 ^a	β-Cp H3 ^b	Cp-H H4 ^c	H1 ^d
<i>cis</i> -2	4.49 (t, <i>J</i> = 2 Hz)	4.42 (t, <i>J</i> = 2 Hz)	4.21 s	7.31 s
<i>trans</i> -2	4.99 (t, <i>J</i> = 3.5 Hz)	4.44 (t, <i>J</i> = 3.5 Hz)	4.31 s	7.05 s
<i>cis</i> -3	4.61 (t, <i>J</i> = 3 Hz)	4.55 (t, <i>J</i> = 3 Hz)	4.25 s	6.24 s
<i>trans</i> -3	5.00 (t, <i>J</i> = 3.25 Hz)	4.57 (t, <i>J</i> = 3.25 Hz)	4.27 s	5.97 s
<i>cis</i> -4		4.46 ^e	4.31 s	5.88 s
<i>trans</i> -4	5.06 (t, <i>J</i> = 3.25 Hz)	4.68 (t, <i>J</i> = 3.25 Hz)	4.31 s	5.78 s
5	5.27 (t, <i>J</i> = 3 Hz)	5.16 (t, <i>J</i> = 3 Hz)	4.47 s	

^a H2 represents protons attached to the α-carbon of substituted cyclopentadienyl ring. ^b H3 represents protons attached to the β-carbon of substituted cyclopentadienyl ring. ^c H4 represents protons attached to the unsubstituted cyclopentadienyl ring. ^d H1 represents a vinylic proton. ^e Overlapped H2 and H3 peaks were resolved by gHMQC and gHMBC spectra.

iodide in 100 mL of diethyl ether was stirred at room temperature for 48 h. After this period of time, the solvent was evaporated and the residue was dissolved in 50 mL of acetone. The resulting solution was poured into 100 mL of a 5% solution of sodium thiosulfate in water. The precipitate was extracted using chloroform, and the organic layer was washed several times with water and dried over sodium sulfate. After the evaporation of chloroform, a solid residue was chromatographed on silica gel using hexane as the eluent. The first yellow-orange fraction was collected, solvent evaporated, and the resulting orange (*E*)-1,2-diiodo-1-ferrocenylethylene, *trans*-2, was recrystallized from hexane. Yield 1.0 g (45%); mp 74–75 °C; ¹H NMR and ¹³C NMR spectra are presented in Tables 1 and 2, respectively; IR (KBr, cm⁻¹): 3064 (Cp–H), 1652 (C=C), 1571 (C=C), 1408, 1255, 1184, 1106, 1039, 1000, 819, 769, 599, 518; Anal. Calcd for C₁₂H₁₀I₂Fe × 0.25 C₆H₁₄: C, 33.40; H, 2.80; found: C, 33.25; H, 2.71. The second yellow-orange fraction produces orange (*Z*)-1,2-diiodo-1-ferrocenylethylene, *cis*-2, which was recrystallized from hexane. Yield 0.6 g (27%); mp 89–90 °C; ¹H NMR and ¹³C NMR spectra are presented in Tables 1 and 2, respectively; IR (KBr, cm⁻¹): 3035 (Cp–H), 1638 (C=C), 1570 (C=C), 1238, 1195, 1103, 1050, 1032, 1000, 929, 805,

Table 2. ^{13}C NMR Peak Assignments in Complexes 2–5

Cmpd.	C1	C2	C3	C4	C5	C6	CN
							
<i>cis</i> -2	84.56	69.94	69.79	70.49	90.32	118.72	
<i>trans</i> -2	73.40	73.06	69.58	70.65	86.27	99.25	
							
<i>cis</i> -3	101.40	70.69	72.05	70.88	84.76	124.15	119.95
<i>trans</i> -3	101.85	72.91	72.03	70.98	82.99	124.29	118.65
							
<i>cis</i> -4	99.91	68.23	73.19	71.02	76.34	135.46	114.16 115.74
<i>trans</i> -4	99.32	69.93	73.16	71.12	74.91	135.06	116.14 116.37
							
5	79.78	72.12	77.79	73.19	75.24	143.98	113.22 113.63 113.74

770; Anal. Calcd for $\text{C}_{12}\text{H}_{10}\text{I}_2\text{Fe} \times 0.25 \text{C}_6\text{H}_{14}$: C, 33.40; H, 2.80; found: C, 34.03; H, 2.58.

(Z)-1-Iodo-2-cyano-1-ferrocenylethylene (*cis*-3) and (Z)-1,2-Dicyano-1-ferrocenylethylene (*cis*-4). A mixture of 0.52 g (1.12 mmol) of (Z)-1,2-diiodo-1-ferrocenylethylene and 0.22 g (2.4 mmol) of CuCN in 10 mL of DMF was stirred in a nitrogen atmosphere for 5 h at 130 °C. After this period of time, the reaction mixture was poured into 100 mL of a 10% solution of aqueous ammonia; the precipitate was filtered, washed several times with water, and dried in air. The deep red solid was dissolved in dichloromethane and chromatographed on silica gel using dichloromethane/hexane (1:1 v/v) as the eluent. The first red-colored fraction was collected, the solvent was evaporated, and the resulting solid was recrystallized from dichloromethane-hexane (1:5 v/v) yielding 0.16 g (39.0%) of *cis*-3. ^1H NMR and ^{13}C NMR spectra are presented in Tables 1 and 2, respectively; IR (KBr, cm^{-1}): 3028 (Cp-H), 2206 (CN), 1635 (C=C), 1571 (C=C), 1408, 1372, 1245, 1106, 1053, 1028, 1000, 816, 791, 777; Anal. Calcd for $\text{C}_{13}\text{H}_{10}\text{INFe}$: C, 43.02; H, 2.78; N, 3.86; found: C, 43.07; H, 2.79; N, 3.83; R_f (SiO_2 , CH_2Cl_2) 0.64; mp 130–131 °C. The second red-violet fraction was collected, the solvent was evaporated under reduced pressure, and the resulting solid was recrystallized from dichloromethane/hexane (1:5 v/v). Yield 0.07 g (24.0%) of *cis*-4. ^1H NMR and ^{13}C NMR spectra are presented in Tables 1 and 2, respectively; IR (KBr, cm^{-1}): 3043 (Cp-H), 2213 (CN), 1635 (C=C), 1574 (C=C), 1457, 1411, 1376, 1277, 1107, 1103, 1078, 1031, 1000, 837, 819, 667; Anal. Calcd for $\text{C}_{14}\text{H}_{10}\text{N}_2\text{Fe}$: C, 64.16; H, 3.85; N, 10.69; found: C, 63.39; H, 3.96; N, 9.97; R_f (SiO_2 , CH_2Cl_2) 0.52; mp 178 °C.

(E)-1-Iodo-2-cyano-1-ferrocenylethylene (*trans*-3) and (E)-1,2-Dicyano-1-ferrocenylethylene (*trans*-4). In full analogy with the preparation of *cis*-3 and *cis*-4, the reaction between 1.0 g (2.15 mmol) of (E)-1,2-diiodo-1-ferrocenylethylene and 0.49 g (5.4 mmol) of CuCN in 15 mL of DMF produces two major reaction products, which were purified by column chromatography. The first red-

colored fraction was found to be complex *trans*-3. Yield 0.33 g (42.5%). ^1H NMR and ^{13}C NMR spectra are presented in Tables 1 and 2, respectively; IR (KBr, cm^{-1}): 3035 (Cp-H), 2199 (CN), 1652 (C=C), 1557 (C=C), 1433, 1408, 1383, 1330, 1202, 1103, 10057, 1003, 996, 809, 805; Anal. Calcd for $\text{C}_{13}\text{H}_{10}\text{INFe}$: C, 43.02; H, 2.78; N, 3.86; found: C, 42.91; H, 2.80; N, 3.80; R_f (SiO_2 , CH_2Cl_2) 0.7; mp 102–103 °C. The second violet fraction, after recrystallization from dichloromethane/hexane (1:5 v/v), gave a pure sample of compound *trans*-4. Yield 0.14 g (25.4%). ^1H NMR and ^{13}C NMR spectra are presented in Tables 1 and 2, respectively; IR (KBr, cm^{-1}): 3062 (Cp-H), 2211 (CN), 1637 (C=C), 1569 (C=C), 1464, 1410, 1383, 1353, 1237, 1210, 1105, 1085, 1037, 1000, 894; Anal. Calcd for $\text{C}_{14}\text{H}_{10}\text{N}_2\text{Fe}$: C, 64.16; H, 3.85; N, 10.69; found: C, 63.75; H, 3.71; N, 10.54; R_f (SiO_2 , CH_2Cl_2) 0.62; mp 80–81 °C.

1,2,2-Tricyano-1-ferrocenylethylene (5).⁶ Tetracyanoethylene (2.56 g, 20 mmol) was added to 20 mL of sulfolane that was preheated to 100 °C and contained 1.86 g (10 mmol) of ferrocene. Immediately after addition, the color of the solution changed first to a green and later to a blue. The reaction mixture was heated with stirring for an additional 10 min, and then it was cooled to room temperature. The resulting solution was poured into 50 mL of water, and the reaction products were immediately extracted using toluene as a solvent. The organic layer was washed several times with water, dried over CaCl_2 , and evaporated to dryness. The blue target compound **5** was purified by column chromatography on silica gel using toluene/hexane (1:3 v/v) as the eluent. Yield: 740 mg (25.8%). mp 130–131 °C (hexane, lit. 125–127,⁷ 134–135⁸); ^1H NMR and ^{13}C NMR are presented in Table 1 and 2; IR (cm^{-1} , KBr): 3100w (Cp-H), 2222s (CN), 1526vs (C=C), 1450s, 1411s, 1381m, 1350m, 1334m, 1294s, 1224m, 1076m, 1044m, 1022m, 998s, 931m, 860m, 825s, 816s, 693s; Anal. Calcd for $\text{C}_{15}\text{H}_9\text{N}_3\text{Fe}$: C, 62.75; H, 3.16; N, 14.64; found: C, 63.13; H, 3.31; N, 14.14.

X-ray Crystallography. X-ray quality single crystals of *cis*-3 and *trans*-3, as well as *cis*-4 and *trans*-4 (CCDC reference numbers 652562–652565) were obtained by slow diffusion of hexane into a saturated CH_2Cl_2 solution of the crude compounds at room temperature followed by a slow evaporation of solvents. Intensity data were collected using a Rigaku AFC-7R diffractometer at room temperature with Mo K α radiation and a graphite monochromator. The raw data were corrected for absorption using a ψ -scan method and processed using the TeXsan 10.3b⁹ program. All structures were solved by the Patterson method and refined by full-matrix least-squares procedures on F^2 using the Crystals for Windows program.¹⁰ The three-parameter Prince-modified Chebychev polynomial weighting scheme incorporated in the program was used for the refinement.

- (7) Freeman, M. B.; Sneddon, L. G. *Inorg. Chem.* **1980**, *19*, 1125.
 (8) Nefedov, V. A.; Bepalov, B. P.; Titov, V. V. *Zh. Org. Khim.* **1974**, *10*, 1553.
 (9) *TeXsan 10.3.b*; Rigaku Inc.: The Woodlands, TX, 1998.
 (10) Betteridge, P. W.; Carruthers, J. R.; Cooper, R. I.; Prout, K.; Watkin, D. J. *J. Appl. Crystallogr.* **2003**, *36*, 1487.
 (11) Frisch, M. J.; Trucks, G. W.; Schlegel, H. B.; Scuseria, G. E.; Robb, M. A.; Cheeseman, J. R.; Zakrzewski, V. G.; Montgomery, J. A., Jr.; Stratmann, R. E.; Burant, J. C.; Dapprich, S.; Millam, J. M.; Daniels, A. D.; Kudin, K. N.; Strain, M. C.; Farkas, O.; Tomasi, J.; Barone, V.; Cossi, M.; Cammi, R.; Mennucci, B.; Pomelli, C.; Adamo, C.; Clifford, S.; Ochterski, J.; Petersson, G. A.; Ayala, P. Y.; Cui, Q.; Morokuma, K.; Malick, D. K.; Rabuck, A. D.; Raghavachari, K.; Foresman, J. B.; Cioslowski, J.; Ortiz, J. V.; Stefanov, B. B.; Liu, G.; Liashenko, A.; Piskorz, P.; Komaromi, I.; Gomperts, R.; Martin, R. L.; Fox, D. J.; Keith, T.; Al-Laham, M. A.; Peng, C. Y.; Nanayakkara, A.; Gonzalez, C.; Challacombe, M.; Gill, P. M. W.; Johnson, B. G.; Chen, W.; Wong, M. W.; Andres, J. L.; Head-Gordon, M.; Replogle, E. S.; Pople, J. A. *Gaussian 98*; Gaussian, Inc.: Pittsburgh, PA, 1998.

Table 3. Crystallographic Data for 3–4

	<i>cis</i> -3	<i>trans</i> -3	<i>cis</i> -4	<i>trans</i> -4
formula	C ₁₃ H ₁₀ N ₁ I ₁ Fe ₁	C ₁₃ H ₁₀ N ₁ I ₁ Fe ₁	C ₁₄ H ₁₀ N ₂ Fe ₁	C ₁₄ H ₁₀ N ₂ Fe ₁
cryst class	orthorhombic	orthorhombic	monoclinic	orthorhombic
space group	<i>P</i> 2 ₁ 2 ₁ 2 ₁	<i>P</i> 2 ₁ 2 ₁ 2 ₁	<i>P</i> 2 ₁ / <i>c</i>	<i>Pbcm</i>
cell params				
<i>a</i> , Å	6.0283(12)	7.7228(13)	11.132(4)	7.6334(15)
<i>b</i> , Å	9.938(2)	11.8209(17)	7.671(5)	13.929(3)
<i>c</i> , Å	20.078(4)	13.2023(19)	13.498(7)	10.926(2)
β , °			92.43(4)	
<i>V</i> , Å ³	1202.8(4)	1205.2(3)	1151.6(10)	1161.8(4)
<i>Z</i>	4	4	4	4
cryst size (mm ³)	0.07 × 0.22 × 0.58	0.08 × 0.12 × 0.61	0.05 × 0.22 × 0.46	0.08 × 0.17 × 0.41
reflms measured	1638	1795	2848	1559
independent reflms	1608	1766	2636	1389
reflms used	1358 ($\sigma \geq 3$)	1502 ($\sigma \geq 3$)	1589 ($\sigma \geq 3$)	980 ($\sigma \geq 3$)
2 θ range (°)	4–55	4–55	4–55	4–55
<i>R</i>	0.0329	0.0439	0.0543	0.0975
<i>R</i> _w	0.0714	0.1048	0.1154	0.2283
no. of params	147	147	154	111
GOF	0.9984	0.9880	0.9108	1.0154

All non-hydrogen atoms were refined anisotropically, while the hydrogen atoms were found in the calculated positions and refined using the riding model. The important crystallographic data on all four complexes are presented in Table 3.

Computational Details. All computations were performed using the Gaussian 03¹¹ software package running under Windows or UNIX OS. Four sets of geometries were used for electronic structure and TDDFT calculations. In the first set, X-ray geometries of complexes *cis*-3, *trans*-3, *cis*-4, *trans*-4, and 5 were used. In the case of the second, third, and fourth sets, all geometries were optimized in vacuum, cyclohexane, or DMSO at DFT level of theory. All solvent media geometry optimizations and TDDFT calculations were conducted using the polarized continuum model (PCM) approach¹² implemented into Gaussian 03 software. The excitation energies were calculated by the TDDFT approach with the lowest 40 singlet excited states being considered. In all calculations, Becke's exchange functional¹³ and Perdew–Wang correlation functional¹⁴ (BPW91) were used. Wachter's full-electron basis set was used for iron, while an SDD effective core potential basis set¹⁵ for iodine, and a 6-311G(d)¹⁶ basis set for all other atoms were used. The percentage of atomic orbital contributions to their respective molecular orbitals was calculated by using the VMOdes program.¹⁷ UV–vis spectra predicted at TDDFT and PCM–TDDFT levels were extracted from Gaussian output files using the SWizard program.¹⁸ Rotational barriers in 2–5 were calculated using a semiempirical PM3 method¹⁹ and gas-phase DFT optimized geometries. In all calculations, the C2–C5–C6–C1 (Table 2) torsion angle was varied in 10° increments.

Results and Discussion

Synthesis and Characterization of Cyanovinylferrocenes.

Cis and *trans* cyanovinylferrocenes 3–4 were

prepared in two steps following chemical transformations presented in Scheme 1 and using commercially available ethynylferrocene, 1, as the starting material. The first reaction involves an electrophilic addition of halogen to a carbon–carbon triple bond similar to that observed earlier for arylacetylenes.²⁰ The presence of a redox-active iron center in 1, however, complicates the electrophilic addition of iodine to the carbon–carbon triple bond. Indeed, in the reaction between 1 and a single equivalent of iodine, only traces of target complexes *cis*-2 and *trans*-2 were found in the reaction mixture. In analogy with the well-known reactions between substituted ferrocenes and iodine,²¹ our observation indicates the formation of [1]⁺I[−] (or most likely [1]⁺I₃[−]) ferricinium-type salts as a result of one-electron oxidation of the iron center in 1. Further increase of the iodine/1 ratio (with an optimum ratio of 2.5:1) in the electrophilic addition reaction leads to the formation of target complexes *cis*-2 and *trans*-2 as the major reaction products with an overall yield of 72%. Both complexes were isolated in a pure form after treatment of the reaction mixture first, with sodium thiosulfate (in order to eliminate excess iodine and reduce ferricinium-type centers to ferrocene-type ones) followed by column chromatography. Interestingly, the iodination reaction of 1 leads to formation of both *cis*-2 and *trans*-2 even in the presence of potassium iodide, while only *trans* isomers were isolated in the case of a similar iodination reaction of substituted alkynes.²⁰ A Rosenmund–von Braun reaction of the individual *cis*-2 and *trans*-2 results in the formation of target *cis* and *trans* 3–4. It was found that this reaction is very sensitive to temperature, reaction time, and the presence of oxygen in the atmosphere. For instance, an increase of the reaction temperature to 152 °C (the boiling temperature of DMF at a pressure of 1 atm) dramatically decreases the total yield of *cis* and *trans* 3 and 4. On the other hand, a decrease in reaction temperature to 100 °C leads to the predominant formation of monosubstituted *cis*-3 and *trans*-3 with a large amount of starting

- (12) Miertus, S.; Scrocco, E.; Tomasi, J. *Chem. Phys.* **1981**, *55*, 117.
 (13) Becke, A. D. *Phys. Rev. A* **1988**, *38*, 3098–3100.
 (14) Perdew, J. P.; Burke, K.; Wang, Y. *Phys. Rev. B* **1996**, *54*, 16533.
 (15) Fuentealba, P.; Preuss, H.; Stoll, H.; Van, Szentpaly, L. *Chem. Phys. Lett.* **1989**, *89*, 418.
 (16) (a) McLean, A. D.; Chandler, G. S. *J. Chem. Phys.* **1980**, *72*, 5639.
 (b) Krishnan, R.; Binkley, J. S.; Seeger, R.; Pople, J. A. *J. Chem. Phys.* **1980**, *72*, 650.
 (17) Nemykin, V. N.; Basu, P. *VMOdes: Virtual Molecular Orbital description program for Gaussian, GAMESS, and HyperChem, Revision A 7.1*; 2003.
 (18) Gorelsky, S. I. *SWizard program*; <http://www.sg-chem.net/>; York University: Toronto, 1998.
 (19) Wolinski, K.; Hinton, J. F.; Pulay, P. *J. Am. Chem. Soc.* **1990**, *112*, 8251.

- (20) (a) Wright, M. E.; Lowe-Ma, C. K. *Organometallics* **1990**, *9*, 347.
 (b) Kabalka, G. W.; Yang, K. *Synth. Commun.* **1998**, *28*, 3807. (c) Fitzgerald, J.; Taylor, W.; Owen, H. *Synthesis* **1991**, 686.
 (21) (a) Neuse, E. W.; Loonat, M. S. *J. Organomet. Chem.* **1985**, *286*, 329. (b) Tebbe, K. F.; Buchem, R. *Z. Anorg. Allg. Chem.* **1998**, *624*, 671.

cis-2 and *trans-2* remaining unreacted. Increase of reaction time to 10 h and the presence of oxygen in the reaction atmosphere results in a dramatic decrease in the yield of target compounds **3** and **4**. The stereoelectronic effect of the ferrocene substituent can be clearly seen from the product distribution in the Rosenmund–von Braun reaction. Indeed, out of four possible monosubstituted products in this reaction, only *cis-3* and *trans-3* were isolated from the reaction mixture, while the other two possible isomers, *cis-6* and *trans-6* (Scheme 1), were not detected in this reaction. Since the Rosenmund–von Braun reaction mechanism can, overall, be described as a copper-supported substitution of a halogen by a cyano group,²² strong electron-donating groups should increase the electron density at the α -vinylic carbon atom and, thus, deactivate the iodine atom toward such a substitution reaction. This is, indeed, in an excellent agreement with the experimental data. Since it was interesting to compare the solvatochromism in cyanovinylferrocenes **3** and **4** with a cyanovinylferrocene bearing a larger number of cyano groups, complex **5** was prepared using the recently optimized tricyanovinyl reaction between ferrocene and tetracyanoethylene.⁶ Complexes **2–5** are colored compounds (*cis-2* and *trans-2* are brown, *cis-3* and *trans-3* are purple, *cis-4* and *trans-4* are violet, and **5** is blue) stable on air in the solid state, but degrade within a few days in polar solvents.

IR spectra of **2–5** reveal characteristic frequencies for valence $\nu_{\text{Cp-H}}$ vibrations observed between 3030 and 3060 cm^{-1} , $\nu_{\text{C=C}}$ vibrations observed at ca. 1630 and 1570 cm^{-1} , and ν_{CN} vibrations (for **3–5**) observed between 2199 and 2213 cm^{-1} , confirming the presence of a vinyl or cyanovinyl group attached to the ferrocene core.

^1H and ^{13}C NMR spectra of **2–5** are presented in Tables 1 and 2, while the typical set of ^1H , ^{13}C , gHMQC, and gHMBC spectra for *trans-3* is shown in Figure SI 1 (Supporting Information). The last two methods were used for the ultimate assignment of signals observed in ^1H and ^{13}C NMR spectra. ^1H NMR spectra of all compounds except *cis-4* consist of three distinct characteristic signals belonging to ferrocenyl protons. The most intense singlet represents protons of the unsubstituted cyclopentadienyl ligand, while two correlating triplets belong to α - and β -protons of the substituted cyclopentadienyl ring. The last two signals are accidentally degenerate (as confirmed by gHMQC spectrum) in the case of *cis-4* and result in a single broad singlet peak in the ^1H NMR spectrum. In addition, the peak corresponding to the vinylic proton can be clearly seen in the 5.7–7.3 ppm region of the ^1H NMR spectra of **2–4** clearly confirming the transformation of the initial ethynyl-type substituent in complex **1** into a vinylic one. This peak monotonically shifts to a higher-field region upon substitution of the iodine atom by the cyanide group in both *cis* and *trans* vinylferrocene derivatives. ^{13}C NMR peak assignments for carbon atoms directly attached to protons in **2–5** were made using respective gHMQC spectra, while gHMBC spectra were used for the identification of the remaining carbon atoms. The position of the peak corresponding to the vinylic carbon atom

Table 4. Oxidation Potentials (Fc/Fc^+) for **2–5** Determined by Cyclic Voltammetry in Acetonitrile/0.1 M TBAP Solution with Scan Rate of 100 mV/s at Room Temperature

compound	oxidation potential mV	peak separation mV
<i>cis-2</i>	137	66
<i>trans-2</i>	153	102
<i>cis-3</i>	237	75
<i>trans-3</i>	257	72
<i>cis-4</i>	314	87
<i>trans-4</i>	332	73
5	484	82

directly attached to the ferrocene group (labeled as C6 in Table 2) is very characteristic and reflects stepwise decrease of its electron density as a function of the increase of the number of cyanogroups in **3–5**. A similar trend was observed for the peaks of carbon atoms that originate from the unsubstituted cyclopentadienyl ring although this effect is less prominent as compared to that observed for the C6 carbon atom (Table 2).

Oxidation potentials of **2–5** were determined using cyclic voltammetry (CV) and are shown in Table 4. In all cases, a single reversible oxidation process, representing $\text{Fe}^{\text{II}}/\text{Fe}^{\text{III}}$ transformation, was observed in the CV curve with typical examples shown in Figure SI 2 (Supporting Information). In agreement with the strong electron-withdrawing character of the cyano group, the oxidation potential monotonically increases as a function of the number of cyano substituents attached to the vinylic group in **2–5** with the largest oxidation potential observed for tricyanovinylferrocene **5**. It is interesting to note that the oxidation potentials of *cis* isomers are always lower (~ 20 mV) than those in respective *trans* isomers.

Molecular Structures of Cyanovinylferrocenes. Crystallographic information on *cis* and *trans* isomers of **3** and **4** is presented in Table 3 and Figure 1, while the most important bond distances and angles are listed in Table 5 along with those for the earlier published **5**.⁶ Crystal structures of the cyanovinyl ferrocenes are extremely rare (less than 10 structures) in the literature,^{4,6,23} and thus, several important features observed in the crystal structures of *cis* and *trans* isomers of **3** and **4** will be discussed below. The iron atom in *trans-4* and **5** along with the two ferrocene carbon atoms were localized at special positions within the crystallographical mirror plane. The cyanovinyl substituents in these complexes are positionally disordered between two sites, which are symmetry related through this plane. In the case of *cis-3*, *trans-3*, and *cis-4*, all atoms were found in nonspecial positions. In all cases, ferrocene is locked in a perfect (*trans-4* and **5**) or slightly distorted (*cis-3*, *trans-3*, and *cis-4*) eclipsed conformation with the largest deviation of $\sim 15.9^\circ$ observed for *cis-3*. The average iron–cyclopentadienyl carbon atom distances were observed in a narrow range (2.034–2.050 Å), which is typical for ferrocene-containing complexes.²³ The average iron–cyclopentadienyl carbon atom bond distances are virtually the same for substituted and unsubstituted cyclopentadienyl rings, sug-

(22) Ellis, G. P.; Romney-Alexander, T. M. *Chem. Rev.* **1987**, *87*, 799.

(23) CCDC database V5.28, November 2006.

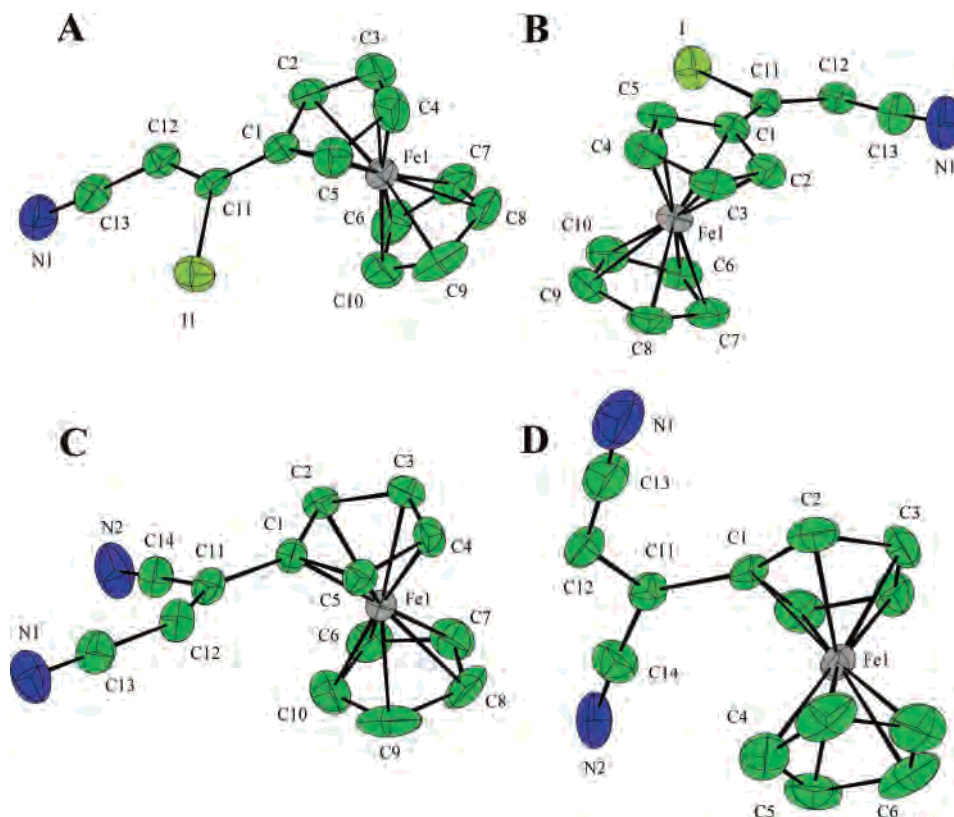


Figure 1. CAMERON graphics of molecular structures of *cis*-3 (A), *trans*-3 (B), *cis*-4 (C), and *trans*-4 (D) at 50% thermal ellipsoids probability. C2, C3, C5, and C6 atoms in the structure of *trans*-4 (D) are symmetry related via a molecular plane, which includes the atoms C1, Fe1, and C4.

Table 5. Selected Bond Lengths (Å) and Angles (deg) in the Structures of 3–5

	<i>cis</i> -3	<i>trans</i> -3	<i>cis</i> -4	<i>trans</i> -4	5 ^e
C1–C11	1.455	1.460	1.458	1.502	1.473
C11–C12	1.332	1.337	1.325	1.325	1.358
C12–C13	1.446	1.440	1.433	1.377	1.425; 1.491
C11–C14 (I1)	2.097	2.115	1.457	1.438	1.453
CN	1.127	1.140	1.138; 1.134	1.145; 1.133	1.095; 1.154; 1.094
Fe–C(Cp) ^a	2.041	2.038	2.034	2.050	2.050
Fe–C(Cp) ^b	2.040	2.034	2.037	2.041	2.040
C12–C11–C14 (I1)	119.63	114.48	118.17	116.08	112.78
C1–C11–C12	123.04	128.83	125.86	122.42	123.48
θ^c	14.14	19.79	19.55	24.84	9.63
α^d	15.89	6.33	8.23	0	0

^a Average Fe–unsubstituted cyclopentadienyl carbon atom distances. ^b Average Fe–substituted cyclopentadienyl carbon atom distances. ^c Θ = torsion angle (see Figure 2). ^d “Skew” angle between two cyclopentadiene ligands, $\alpha = 0^\circ$ for eclipsed conformation (see Figure 2). ^e Room-temperature structure from ref 6.

gesting that the presence of the electron-withdrawing cyanovinyl group in one of the two cyclopentadienyl rings has little influence on iron–cyclopentadienyl ring interactions (Table 5). In all complexes studied, the carbon–carbon double bond was clearly observed between carbon atoms in the vinyl group. In addition, the sp^2 character of these atoms can clearly be seen from the planarity of the cyanovinyl group and the close to 120° angles between the substituents and the C=C bond. The observed torsion angle, θ , between the substituted cyclopentadienyl ring and the cyanovinyl group varies from 9.6° to 24.8° (Table 5) and is still smaller than that found in (octamethylferrocenylmethylene)malononitrile in which the torsion angle between the ferrocene core and the dicyanovinyl substituent varies from 37° and 41° . Such a difference can originate either from the crystal packing forces or steric interactions between the

cyanovinyl group and the ferrocene core. In order to clarify this point, rotational barriers of the substituted vinyl group in 2–5 were calculated at the semiempirical PM3 level, and the results are presented in Figure 4. The calculated rotational barrier energy profiles for all *trans* isomers of 2, 3, and 4, as well as the tricyanovinyl 5, reveal two distinct peaks corresponding to conformations presented in Figure SI 3 (Supporting Information), while those in *cis* isomers of 2, 3, and 4 have only a single significant rotational barrier because of the different orientation of the iodine or cyano substituent at the β -carbon of vinyl group. The calculated rotational energy profiles clearly suggest that rotational barriers for cyanovinyl groups are low in a large range of torsion angles, and thus, the observed differences for 3–5 can, probably, be attributed to the differences in crystallographic packing forces.

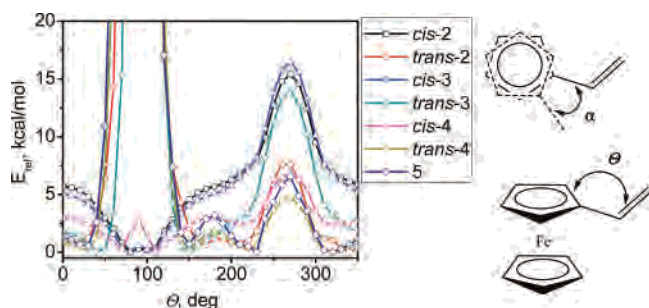


Figure 2. Rotational barrier energy profiles for 2–5 calculated at the PM3 level (all geometries were optimized at DFT level as described in the Experimental Section). Definitions of angle, α , and torsion angle, θ , are given on the diagram.

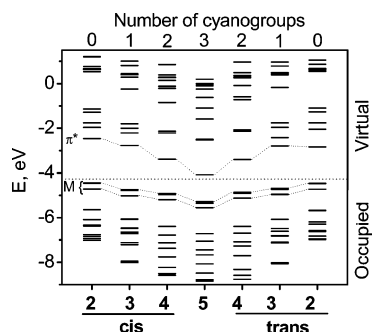


Figure 3. Molecular orbital diagram for 2–5 calculated for the gas phase optimized at DFT level geometries.

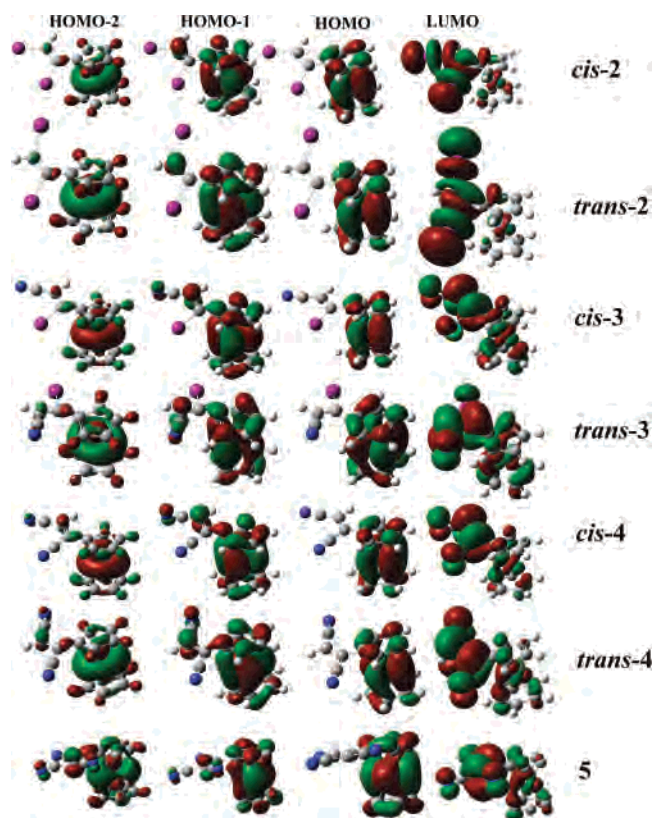


Figure 4. Frontier orbitals calculated for 2–5 in the gas phase at the DFT level.

Electronic Structures of Cyanovinylferrocenes. In order to gain an insight into the electronic structure, solvatochromism, and UV–vis spectra of 2–5, we conducted DFT calculations on the systems of interest. The molecular orbital

diagram for 2–5 is shown in Figure 3, while the molecular orbital compositions calculated at the DFT level are presented in Table 6. All complexes reveal several common features. First, the HOMO in all cases predominantly consists of an iron d_{xy} atomic orbital coupled with cyclopentadienyl π orbitals. The HOMO is closely placed to the predominantly iron-centered $d_{x^2-y^2}$ (HOMO-1) and d_{z^2} (HOMO-2) orbitals (Figure 4). These three orbitals are energetically well-separated from the other occupied molecular orbitals (Figure 3). The energy of the HOMO monotonically decreases when the number of cyano groups attached to the vinyl substituent increases, reflecting the electron-withdrawing nature of the cyano groups and in excellent agreement with the NMR spectra (Tables 1 and 2). In all cases, the LUMO consists of a π -orbital predominantly localized on the vinyl-containing fragment, while predominantly metal-centered d_{xz} and d_{yz} orbitals were found at higher energies (Figure 3). The presence of the ligand-based low-energy π -orbital is responsible for creating the possibility of low-energy metal-to-ligand charge-transfer (MLCT) bands observed in the UV–vis spectra of 2–5, which are discussed below on the basis of TDDFT calculations. It is interesting to note that the calculated energies of the HOMO in the gas-phase for cis and trans isomers of 3 and 4 are in disagreement with the experimental electrochemical data. Indeed, the DFT predicted energies of the HOMO suggest that the oxidation potential of trans isomers of 3 and 4 should be lower as compared to that in respective cis isomers (Table 6). The calculated energies of the HOMO in polar solvent, however, are in excellent agreement with the experimental data, suggesting that the role of the solvent should not be ignored in the DFT predicted oxidation potentials of cis and trans 2–4 (Table 6).

UV–Vis and MCD Spectra, Solvatochromic Properties, and TDDFT and TDDFT/PCM Results on Cyanovinylferrocenes. The UV–vis and MCD spectra of 2–5 are presented in Figure 5, while band positions and intensities are listed in Table 7. In all cases, the most intense band in the UV–vis spectra was observed between 284 and 365 nm. The energy of this band monotonically increases as the number of cyano groups decreases in respective complexes. Indeed, it is located at 365 nm in 5, \sim 312 nm in cis and trans isomers of 4, \sim 300 nm in cis and trans isomers of 3, and \sim 285 nm in cis and trans isomers of 2. A similar trend was also observed for the lowest energy transition observed at 642 nm in 5, \sim 540 nm in cis and trans isomers of 4, \sim 485 nm in cis and trans isomers of 3, and \sim 469 nm in cis and trans isomers of 2 (Figure 5). In addition, in the case of 2–4, a band located between the intense UV transition and the lowest energy one was observed in the UV–vis spectra. Finally, in the case of 3–5, an additional band between 250 and 270 nm was observed. The room-temperature MCD spectra of 2–5 consist of very weak signals. These spectra, however, reveal several common features that are helpful for the band assignments presented below. The most intense signal in the MCD spectra is the negative Faraday B -term, which in all cases corresponds to the most intense band in UV–vis spectra.

Table 6. Atomic Orbitals Contribution into MOs in Complexes 2–5^a

orbital no.	energy, (eV)	iron	ferrocene	vinyl substituent	energy, (eV)	iron	ferrocene	vinyl substituent
cis-2				trans-2				
58	-5.638	5.5	28	72	-5.675	3.9	20.3	79.7
59	-4.723	86.4	97.9	2.1	-4.731	86.1	97.7	2.3
60	-4.46	59.1	96.9	3.1	-4.476	58.1	96.8	3.2
61	-4.449 (-4.378)	62.3	98.2	1.8	-4.462 (-4.419)	63.6	98.7	1.3
62	-2.464	3.5	8.4	91.6	-2.836	1.7	4.3	95.7
63	-1.963	23.9	52.2	47.8	-2.042	27.9	57.8	42.2
64	-1.757	42.1	94.4	5.6	-1.755	43	96.2	3.8
65	-1.28	10.2	35.7	64.3	-1.269	10.3	36.3	63.7
cis-3				trans-3				
61	-6.068	5.5	32.8	67.2	-6.074	4.9	35.2	67.2
62	-5.019	86.3	97.9	2.1	-4.96	86.1	97.7	2.1
63	-4.783	58.7	97.1	2.9	-4.735	59.7	97.1	2.9
64	-4.748 (-4.557)	64.1	98.6	1.4	-4.689 (-4.570)	64.6	99	1.4
65	-2.772	19.3	38.7	61.3	-2.792	17.6	34.9	61.3
66	-2.212	5.4	15.8	84.2	-2.418	1.4	7.8	84.2
67	-1.996	28.2	63.2	36.8	-1.954	41.9	92.8	36.8
68	-1.798	31.7	82.3	17.7	-1.757	33.1	83.7	17.7
cis-4				trans-4				
64	-6.39	6.2	58.4	41.6	-6.388	5.9	61.8	38.2
65	-5.196	85.9	97.4	2.6	-5.128	85.5	97	3
66	-4.974	59.1	96.6	3.4	-4.909	60.6	96.7	3.3
67	-4.929 (-4.658)	65.1	99.2	0.8	-4.86 (-4.660)	65.5	99.2	0.8
68	-3.381	12.4	23.8	76.2	-3.403	11.6	24.1	75.9
69	-2.211	44.5	99.2	0.8	-2.131	44.8	99.4	0.6
70	-2.13	39.9	92.8	7.2	-2.074	40.5	93	7
71	-0.845	1.7	28.9	71.1	-0.715	1.1	18.9	81.1
5								
70	-6.716	5.9	54.1	45.9				
71	-5.551	82.8	95.2	4.8				
72	-5.35	61.2	95.9	4.1				
73	-5.288 (-4.959)	66.4	99.3	0.7				
74	-4.078	13.3	25.5	74.5				
75	-2.525	44.9	99.3	0.7				
76	-2.492	41	93.7	6.3				
77	-1.587	1.3	10	90				

^a Optimized gas-phase geometries; HOMO highlighted in bold and LUMO highlighted in bold/italic fonts, respectively. Energies of HOMO calculated in DMSO are presented in parenthesis. All orbitals have an “A” symmetry.

Another negative Faraday *B*-term represents the highest energy band observed ca. 260 nm in the UV–vis spectra of **3–5**. The lowest energy transition observed in the UV–vis spectra of **2–5** corresponds to the lower energy positive Faraday *B*-term and the higher energy negative Faraday *B*-term observed in the MCD spectra centered close to the observed UV–vis spectrum maximum (Figure 5). In addition, a positive Faraday *B*-term was observed for **2–5** between 374 and 405 nm with maxima close to those observed for the respective bands in the UV–vis spectra.

TDDFT calculations proved to be accurate in the prediction of vertical excitation energies in inorganic and organometallic compounds,²⁴ and thus, this approach was used to aid in the understanding of UV–vis and MCD spectra of **2–5**. The TDDFT-predicted gas-phase vertical excitation energies for **3–5** are shown in Figure 6 and Table SI 1 (Supporting Information). An excellent agreement between calculated vertical excitation energies and the absorption bands observed in the UV–vis and MCD spectra was obtained in all cases. Such a good agreement allows us to

accurately assign experimentally observed bands to the specific transitions discussed below. DFT calculations of the electronic structure of **2–5** suggest the presence of three closely spaced predominantly metal-centered orbitals in the HOMO-to-HOMO-2 region and a predominantly ligand-based LUMO (Table 6). In agreement with this general electronic structure description, three MLCT transitions with predominantly HOMO → LUMO (band 1), HOMO-1 → LUMO (band 2), and HOMO-2 → LUMO (band 3) contributions were predicted in the low-energy region of the UV–vis spectra of **2–5** in the gas phase using the TDDFT method (Table SI 1, Figure 6). These three transitions form the broad, intense low-energy MLCT band observed in the UV–vis spectra of **2–5**. The predominant MLCT character of these transitions is in excellent agreement with the appreciable solvatochromism of the low-energy band experimentally observed in **2–5**. Next, several bands predicted by TDDFT calculations belong to low-intensity, predominantly d–d transitions. On the other hand, the most intense band observed between 284 and 365 nm in UV–vis and MCD spectra of these compounds does, probably, predominantly consist of several overlapping π – π^* transitions from occupied π orbitals of the ferrocene ligand to the LUMO as predicted by TDDFT calculations. Predominant π – π^* character of these transitions is in excellent agreement with

(24) (a) Nemykin, V. N.; Olsen, J. G.; Perera, E.; Basu, P. *Inorg. Chem.* **2006**, *45*, 3557. (b) Nemykin, V. N.; Basu, P. *Inorg. Chem.* **2003**, *42*, 4046. (c) Seth, M.; Ziegler, T. *J. Chem. Phys.* **2005**, *123*, 144105/1. (d) Wang, F.; Ziegler, T. *J. Chem. Phys.* **2005**, *122*, 074109/1. (e) Maji, S.; Patra, S.; Chakraborty, S.; Janardanan, D.; Mobin, S. M.; Sunoj, R. B.; Lahiri, G. K. *Eur. J. Inorg. Chem.* **2007**, 314.

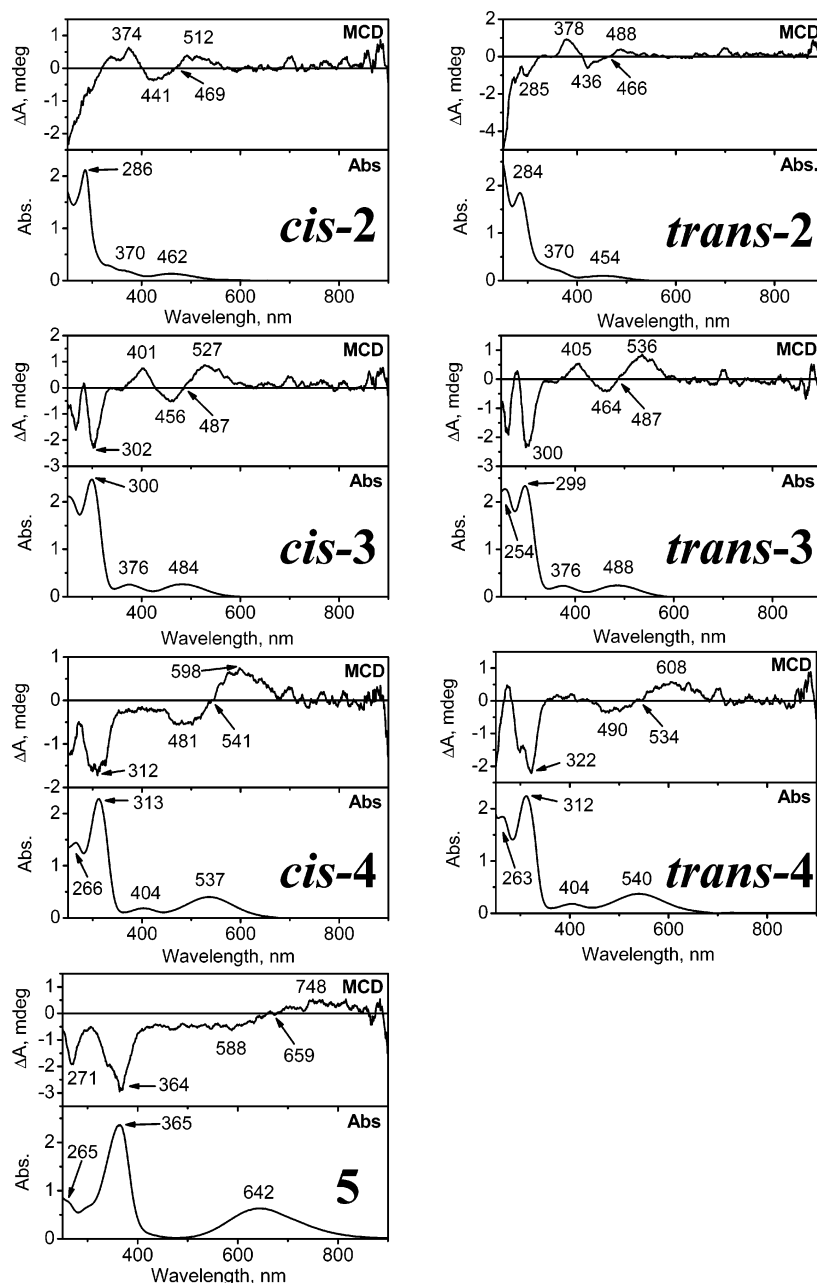


Figure 5. Room-temperature UV-vis and MCD spectra of **2–5** in dichloromethane (in all cases the concentration of sample is ca. 2×10^{-4} mol/L).

Table 7. Room-Temperature UV-Vis Spectra of **2–5** in Dichloromethane

complex	λ (ϵ , L mol ⁻¹ cm ⁻¹)
<i>cis-2</i>	286 (10200), 370sh, 462 (650)
<i>trans-2</i>	284 (10300), 370sh, 454 (600)
<i>cis-3</i>	252 (10000), 300 (11700), 376 (1200), 484 (1250)
<i>trans-3</i>	258 (11700), 299 (12000), 376 (1200), 484 (1250)
<i>cis-4</i>	266 (7250), 313 (11500), 404 (950), 537 (2000)
<i>trans-4</i>	263 (9400), 312 (11400), 404 (900), 540 (1900)
5	265 (3400), 365 (11000), 642 (2900)

the small solvatochromism of the 284–365 nm band experimentally observed in **2–5**. Since the X-ray geometries for *cis* and *trans* isomers of **2** are not available, we also conducted TDDFT calculations on **2–5** using DFT-optimized geometries. The TDDFT results for this set of calculations are presented in Supporting Information tables and, when comparison with TDDFT calculations on X-ray geometries

are available, provide a good qualitative agreement. All transition energies calculated for the optimized geometries, however, are underestimated in comparison to experimental and TDDFT-predicted vertical excitation energies for X-ray geometries.

One of the most interesting features of **2–5** is that the low-energy optical transition has significant solvatochromic behavior with the maximum observed solvatochromic shift of 1331 cm^{-1} for *cis-4* (Figure 7). The observed solvatochromic effect for *cis-4* and **5** is about twice as large in comparison to that found in (octamethylferrocenylmethylene)malononitrile⁴ and is comparable to the solvatochromic shift in the 2-nitro-3-(octamethylferrocenyl)acrylonitrile.³ The most intense, high-energy band located at ca. 360 nm, on the other hand, shows little solvatochromism, confirming its predominantly $\pi-\pi^*$ nature. The electronic absorption

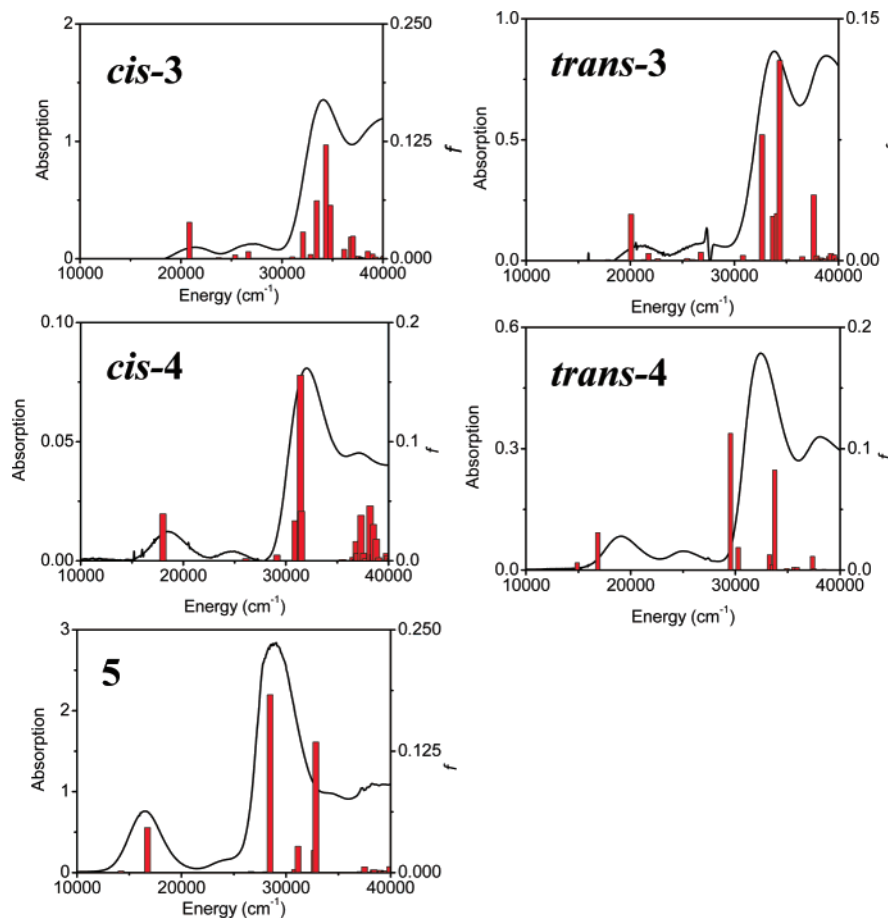


Figure 6. TDDFT-predicted (solid bars) gas-phase vertical excitation energies of 3–5 as compared to experimental UV–vis data (hexane). X-ray geometries of respective complexes were used in all TDDFT calculations.

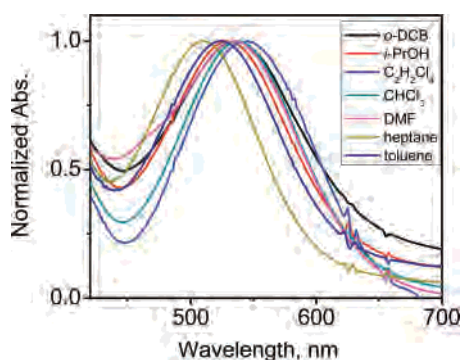


Figure 7. Normalized UV–vis spectra of *cis*-4 in the low-energy MLCT band region.

spectra of 2–5 in 20 standard protic and aprotic solvents of different polarity are summarized in Table 8.

We attempted to correlate the experimentally observed energy of the low-energy band in *cis* and *trans* isomers of 2–4 (similar correlations for 5 were discussed in ref 6) with various empirical solvent parameters and experimentally derived constants. The solvents scales such as Kosower's Z ,²⁵ Reichardt's $E_T(30)$ MLCT,²⁶ Gutmann's AN and DN,²⁷ dipole moment of solvents,²⁸ Swain's *Acity* and *Basity*

parameters,²⁹ and Eisenberg's empirical Pt(NN)(SS)³⁰ gave considerably weak correlations with experimental data for *cis* and *trans* isomers of 2–4.

We also attempted to correlate the observed MLCT band position with the Kamlet–Taft model, which was found to be very useful in explanation of the solvatochromic properties of donor–acceptor ferrocene-based assemblies:³¹

$$E(\text{cm}^{-1}) = E^\circ + s(\pi^* + d\delta) + a\alpha + b\beta \quad (1)$$

$$E(\text{cm}^{-1}) = E^\circ + s\pi^* + a\alpha + b\beta \quad (2)$$

$$E(\text{cm}^{-1}) = E^\circ + s\pi^* + a\alpha \quad (3)$$

where E° , s , d , a , and b are the coefficients determined from regression analysis, α is the hydrogen-bond donation ability of the solvent, while β is the hydrogen-bond acceptance ability of the solvent; π^* is a parameter that describes the polarity and polarizability of the solvent, and the δ term, which is dependent on the class of solvent to be studied as defined by Taft. Often, the contribution from the last term is negligibly small, which leads to the modified Kamlet–Taft expression shown in eq 2.²⁷ Recently, it has also been

(25) Kosover, E.; *J. Am. Chem. Soc.* **1958**, *80*, 3253.

(26) Reichardt, C. *Angew. Chem., Int. Ed. Engl.* **1965**, *4*, 29.

(27) Marcus, Y. *Chem. Soc. Rev.* **1993**, 409.

(28) *The Merck Index*, 14th ed.; Merck Publishing Inc.: Rahway, NJ, 2006.

(29) Swain, C. G.; Swain, M. S. *J. Am. Chem. Soc.* **1983**, *105*, 502.

(30) Cummings, S. D.; Eisenberg, R. *J. Am. Chem. Soc.* **1996**, *118*, 1949.

(31) Kamlet, M. J.; Abboud, J.-L. M.; Taft, R. W. *J. Am. Chem. Soc.* **1977**, *99*, 6027.

Table 8. UV–Vis Maxima for the Lowest Energy Band (cm^{-1}) in **2–5** in Different Solvents along with the Solvent Parameters and Transition Energies

solvent ^a	α	β	π^*	<i>cis</i> - 2	<i>trans</i> - 2	<i>cis</i> - 3	<i>trans</i> - 3	<i>cis</i> - 4	<i>trans</i> - 4	5
hexane	0	0	−0.04	22124	21930	21459	20964	19646	19084	16529
heptane	0	0	−0.08	22026	21978	21413	20964	19608	19048	16474
cyclohexane	0	0	0	22026	21930	21322	20920	19531	18939	16447
diethylether	0	0.47	0.27	22173	22173	21459	20920	19231	18975	16077
toluene	0	0.11	0.54	22026	21692	21097	20790	19120	18762	15948
ethylacetate	0	0.45	0.55	21978	21882	20964	20619	19084	18904	15898
THF	0	0.55	0.58	22026	21739	20877	20833	19048	18762	15848
2-propanol	0.76	0.84	0.48	21692	21645	20920	20534	18868	18519	15823
1,2-dimethoxyethane	0	0.41	0.53	21739	21786	20877	20833	18975	18939	15773
acetone	0.08	0.43	0.71	21882	21739	20833	20661	18832	18762	15773
methanol	0.98	0.66	0.6	21552	21505	20877	20492	18797	18727	15748
ethanol	0.86	0.75	0.54	22272	22222	20747	20661	18904	18797	15748
butyronitrile	0	0.4	0.71	21834	21786	21142	20747	18832	18762	15699
DMF	0	0.69	0.88	21882	22075	20619	20576	18727	18692	15625
acetonitrile	0.19	0.4	0.75	21786	21645	20833	20747	18692	18727	15600
chloroform	0.2	0.1	0.58	21834	21692	20661	20619	18622	18248	15600
dichloromethane	0.13	0.1	0.82	22075	21978	20747	20576	18519	18315	15552
<i>o</i> -dichlorobenzene	0	0.03	0.8	21645	21692	20661	20534	18657	18450	15552
DMSO	0	0.76	1	21645	22321	20619	20661	18553	18657	15480
1,1,2,2-tetrachloroethane	0	0	0.95	22129	21786	20619	20661	18315	18182	15244
solvatochromism, cm^{-1}				720	816	840	472	1331	902	1285
Δ TDDFT/PCM, cm^{-1} ^b				753	336	909	895	1324	807	456

^a Solvent parameters are taken from ref.27. ^b Solvatochromic effect calculated between hexane and DMSO solutions for the most intense component (band 3) in the low-energy transition.

suggested²⁷ that in the case of substituted vinylferrocenes, the hydrogen-bond acceptance parameter β is negligibly small and can be ignored in the regression analysis (eq 3), and thus, solvatochromic properties of these compounds can be predicted on the basis of the parameters π^* and α . Surprisingly, only *cis*-**4** and **5** show good correlation within the borders of the Kamlet–Taft model (Table SI 2, Supporting Information), thus indicating a more complex nature of solvent–solute interaction in these assemblies. In order to account for solvent–solute interactions, TDDFT/PCM calculations on **2–5** were conducted with hexane and DMSO as solvents. The magnitude of TDDFT/PCM-predicted solvatochromic properties of complexes **2–5** agrees well with experimental data on a qualitative level (Table 8), suggesting the usefulness of the TDDFT/PCM approach for the estimation of solvatochromism in ferrocene-based donor–acceptor assemblies.

Conclusions

Cis and trans isomers of ferrocene-based donor–acceptor complexes, $\text{Fc}-\text{C}(\text{I})=\text{CH}(\text{I})$, $\text{Fc}-\text{C}(\text{I})=\text{CH}(\text{CN})$, and $\text{Fc}-\text{C}(\text{CN})=\text{CH}(\text{CN})$, along with the $\text{Fc}-\text{C}(\text{CN})=\text{C}(\text{CN})_2$ complex earlier described by us have been prepared and characterized by ¹H, ¹³C, gHMQC, and gHMBC NMR approaches, IR, UV–vis, and MCD spectroscopy methods, as well as elemental analyses. The oxidation potentials investigated by cyclic voltammetry are in agreement with the electron-acceptor strength of substituents attached to the

ferrocene core. X-ray crystallography of *cis* and *trans* isomers of $\text{Fc}-\text{C}(\text{I})=\text{CH}(\text{CN})$ and $\text{Fc}-\text{C}(\text{CN})=\text{CH}(\text{CN})$ reveal significant rotational flexibility of the cyanovinyl group, which was explained on the basis of semiempirical PM3 calculations. The electronic transitions observed in UV–vis spectra of all compounds were assigned on the basis of UV–vis and MCD spectra and TDDFT calculations. The electronic structure and solvatochromic properties in all complexes were investigated by UV–vis spectroscopy and TDDFT approaches. The calculated vertical excitation energies and magnitudes of solvatochromic effect are consistent with the experimental data and clearly suggest the dominance of MLCT bands in the visible region of the UV–vis spectra for all complexes.

Acknowledgment. Generous support from the Research Corporation (Cottrell College Science Award CC6766), University of Minnesota Grant-in-Aid (Grant No. 20209) and Minnesota Supercomputing Institute to V.N. and University of Minnesota Duluth Undergraduate Research Opportunity Grants to J.G. and R.H. are greatly appreciated.

Supporting Information Available: Crystallographic data for *cis* and *trans* isomers of **3–5** in CIF format; tables of DFT and TDDFT calculated energies, and full molecular orbital compositions for **2–5**; and solvatochromic correlation analysis within the Kamlet–Taft model for **2–5**. This material is available free of charge via the Internet at <http://pubs.acs.org>.

IC700558V